Journal of Zhejiang University-SCIENCE A (Applied Physics & Engineering)
ISSN 1673-565X (Print); ISSN 1862-1775 (Online)
www.zju.edu.cn/jzus; www.springerlink.com
E-mail: jzus@zju.edu.cn

A numerical method for analyzing the permeability of heterogeneous geomaterials based on digital image processing*

Long YAN[1], Qing-xiang MENG[†‡1,2], Wei-ya XU[1], Huan-ling WANG[1,3],
Qiang ZHANG[1,4], Jiu-chang ZHANG[1], Ru-bin WANG[1]
(*[1]Key Laboratory of Ministry of Education for Geomechanics and Embankment Engineering, Hohai University, Nanjing 210098, China*)
(*[2]Department of Civil & Environmental Engineering, University of Waterloo, Waterloo N2L 3G1, Canada*)
(*[3]Key Laboratory of Coastal Disaster and Defense of Ministry of Education, Hohai University, Nanjing 210098, China*)
(*[4]Department of Civil Engineering, University of Toronto, Toronto M5S 1A4, Canada*)
[†]E-mail: tianyameng@hhu.edu.cn

Received Dec. 15, 2015; Revision accepted July 13, 2016; Crosschecked Jan. 5, 2017

Abstract: In this study, we propose a digital image processing technology for estimating the macro permeability property of heterogeneous geomaterials. The technology is based on a connected-component labeling algorithm and provides a novel and effective method for geometry vectorization and microstructure identification. A color photo of a soil and rock mixture (SRM) is taken as an example. Information about the distribution of aggregate and a vectorgraph, which can be used in numerical analysis, are obtained automatically. A numerical permeability test is carried out to estimate the macro permeability coefficient of the heterogeneous medium. The effects on macro permeability of three parameters, scale dependency, material heterogeneity and the rock fraction, are discussed. The results indicate that the SRM has a scale dependent property and the representative element volume (REV) length is about six times the maximum major axis of the aggregate. The heterogeneity parameter has a major effect on macro permeability characteristics within a certain range. There is a weak tendency for the macro permeability to decrease as the rock fraction increases. Although the rock fraction is not the only factor, it does have an influence on the macro permeability. We conclude that the novel method developed in this study has good prospects for widespread application in macro parameter estimation and related research fields.

Key words: Heterogeneous geomaterials; Digital image processing (DIP); Macro permeability coefficient; Scale dependency
http://dx.doi.org/10.1631/jzus.A1500335 **CLC number:** TV512

1 Introduction

Permeability is an important component of the physical characteristics of geomaterials and is intimately associated with their mesostructure. However, identifying the permeability of heterogeneous geomaterials in a real project often needs in-site tests which are likely to require a great deal of human effort and material resources. Hence, it is of great value to establish a numerical model for the purpose of examining permeability, which can help recognize the mesostructure of heterogeneous geomaterials.

Digital image processing (DIP) is a new technology commonly used for converting digital pictures into a vectorization form and extracting significant information through various mathematical algorithms. It has been widely used in engineering, computer science, information science, statistics, physics, and other disciplines (Xu *et al.*, 2008b;

---

‡ Corresponding author

* Project supported by the National Natural Science Foundation of China (Nos. 11272113, 51479049, and 51679069) and the Jiangsu Provincial Natural Science Foundation of China (No. BK2012809)

ORCID: Long YAN, http://orcid.org/0000-0001-6099-5925; Qing-xiang MENG, http://orcid.org/0000-0002-8771-5177

Steinberg *et al.*, 2010; Zeng *et al.*, 2013; Chaves *et al.*, 2015). Geomaterials are typically heterogeneous materials with complex microstructures. With the application of DIP techniques, information about these internal heterogeneities or microstructures (such as cracks on a material surface, the shapes of components, and the distribution of different ingredients) can be extracted in a quantitative form (Johnson *et al.*, 2002). In addition, the development of computational methods has led to the production of several powerful numerical tools for the simulation of geomaterials, including finite difference method (FDM), finite element method (FEM), and discrete element method (DEM). Within the past two decades, the incorporation of DIP into computational methods has been reported to be efficient in the analysis of these heterogeneous materials (Chen *et al.*, 2005; Yu *et al.*, 2007; Bessa *et al.*, 2012; Carroll *et al.*, 2013).

Information about the incorporation of DIP into the analysis of the permeability of heterogeneous geomaterials is very limited. This paper proposes an innovative DIP method and a general framework for seepage analysis.

Geomaterials such as soil, rock, and concrete are either natural or artificial. These materials normally comprise soil, gravel, cement, and voids and cracks. Each individual component is distributed in geomaterials in a stochastic manner following a specific distribution like exponent or normal types. The individual ingredients feature different physical and mechanical properties (such as density, porosity, and Young's modulus). The responses of components of geomaterials under internal and external loading are variable, and interactions among these individual components are complicated. Physical and mechanical properties (such as the fracture model, crack propagation, and constitutive equation) of geomaterials tend to depend on the internal mesostructure including the distribution, shape, and proportion of each component. It has been well recognized that heterogeneities and mesostructure are of great significance to the physical and mechanical properties of geomaterials.

As a crucial parameter of the physical properties of geomaterials, the permeability coefficient is widely used in geotechnical engineering. In laboratories, the coefficient of permeability is often estimated from flow velocity and water pressure for conventional materials (Venkatramaiah, 2006). For low permeability media, the pulse method is usually used to measure gas permeability (Skoczylas and Henry, 1995; Xu *et al.*, 2009). However, these tests are limited by the scale of specimens, and the laboratory scale is different from the *in-situ* field scale (Zhou *et al.*, 2006; Xu *et al.*, 2009). In engineering practice, large-scale field tests are likely to be required. *In-situ* tests tend to consume a large number of manpower and resources. Thus, numerical models to analyze heterogeneous geomaterials on a large scale are urgently required.

Conventional seepage analysis assumes geomaterials are homogeneous or piecewise homogeneous, which generally ignores the effects of mesostructure (Mariño and Luthin, 1982; Rushton, 2004). To consider the effects of heterogeneities and microstructures, many recent studies have analyzed the behavior of geomaterials. These studies can be classified into two approaches. The first approach is to preset values in terms of the sizes, shapes, and distribution of different components (Bažant *et al.*, 1990; Kwan *et al.*, 1999a; Wang *et al.*, 1999; Yue *et al.*, 2003; Chena *et al.*, 2013; Wang *et al.*, 2015). In particular, Bažant *et al.* (1990) proposed a take-and-place technique to simulate spherical aggregate particles in the computation of fractures. Kwan *et al.* (1999a) and Wang *et al.* (1999) generated a random aggregate structure in which the shape, size, and distribution of aggregate particles resembled real concrete in a statistical sense, and carried out a mesoscopic study of concrete. This method describes the geometrical heterogeneity of geomaterials and has shown that microstructure plays an important role in the behavior of geomaterials. Though the presumptions of the internal properties of geomaterials may represent the heterogeneity and microstructure of geomaterials from a statistical view, there are still differences compared with the *in-situ* aggregate distribution, case by case. The second approach is to obtain the real mesostructure using techniques like digital imaging, computer tomography (CT), and nuclear magnetic resonance (NMR). Because of its simplicity and convenience for identifying surface microstructures, DIP has been widely used for capturing morphological characteristics in engineering, information science, statistics, physics, and other disciplines (Yue *et al.*, 1995; Kwan *et al.*, 1999b; Ammouche *et al.*, 2000; Kameda, 2004; Xu J.M. *et al.*, 2007; Kemeny *et al.*, 2010; Yu *et al.*, 2012; Li *et al.*, 2014; Khan *et al.*, 2015). For example, Kameda (2004) established a digital rock approach to analyze the evolution of permeability in sandstone. Further progress has been made in the incorporation of DIP techniques into numerical methods (Chen *et al.*, 2004; 2005; 2007; Yue *et al.*, 2004; Yu *et al.*, 2006; Zhu *et al.*, 2006; Xu W.J. *et al.*, 2007; 2008a; 2008b; Armesto *et al.*, 2009; Michailidis *et al.*, 2010). Yue *et al.* (2004) successfully carried out quantitative analysis of heterogeneity and proposed a digital image processing based finite element method (DIP-FEM) for asphalt concrete. Chen *et al.* (2004) analyzed the failure behavior of heterogeneous rock based on DIP. Yu *et al.* (2006) established a multi-scale coupled numerical model based on DIP and simulated the failure process of concrete under uniaxial loading.

Literature reviews indicate that the DIP technique is an effective tool in quantitative analysis as it provides an explicit representation of the heterogeneity and microstructure of geomaterials. Considering there are few studies combining DIP with seepage analysis, the main objective of this study was to present a novel method for the analysis of the permeability of geomaterials. Specifically, DIP technology is used in the quantification of the distribution of different components and the extraction of boundaries. Results from DIP are used to generate automatically particles that can be imported into conventional numerical software packages. A general flowchart of the main techniques and implementation procedures is shown in Fig. 1. The rest of this paper is organized as follows: First, we will give a brief introduction to DIP, including data formatting of digital images and pre-treatment techniques. Second, a DIP method for geomaterials based on the connected-component labeling algorithm will then be presented and a detailed example of implementation of this method will be given showing the conversion of a digital image from an original figure to a vectorial drawing. Afterwards, we will use related algorithms to generate the finite element mesh automatically from the vectorized images. (4) Finally, we will incorporate the grid into FEM software packages and analyze the property of permeability based on numerical tests.

2 Pre-treatment techniques for soil and rock mixture

Before numerically modeling a photo of geomaterials, the pre-treatment of the image is very important. Digital photographs captured by a digital camera or scanner consist of a rectangular matrix of image elements or pixels. Note that the formats of gray images and colored images are different. For gray level images, each pixel is represented by a value with an integer interval from 0 to 255 (gray images) or from 0 to 1 (binary images). Hence, digital images containing $m\times n$ pixels can be represented by a discrete function $f(i,j)$ in the i and j Cartesian coordinate system (Yue *et al.*, 2003):

$$\text{digital image} = f(i,j) = \begin{bmatrix} f(1,1) & f(1,2) & \cdots & f(1,m) \\ f(2,1) & f(2,2) & \cdots & f(2,m) \\ \vdots & \vdots & & \vdots \\ f(n,1) & f(n,2) & \cdots & f(n,m) \end{bmatrix}, \tag{1}$$

where i ranges from 1 to n and j from 1 to m.

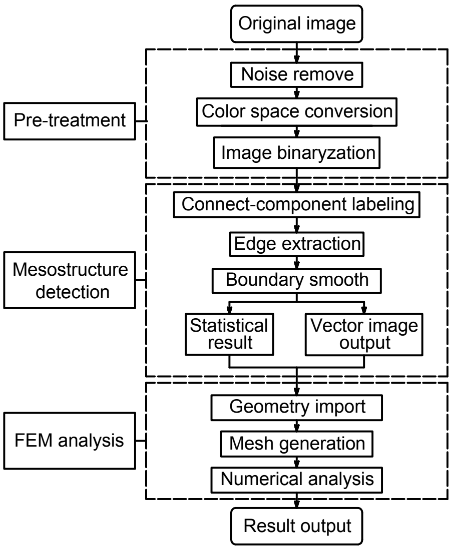

Fig. 1 General flowchart for DIP-based analysis of the permeability of heterogeneous media

As for a gray level graph, Yue *et al.* (2003) have presented a detailed implementation of the pre-treatment method. For color images, there are three integer values at each pixel to represent different parts of red, green, and blue. As a result, the data of color images can be expressed as a function $f_p(i, j)$, where p=1, 2, 3. In this study, a photo of a soil and rock mixture (SRM) is taken as an example (Fig. 2). This image was generated with a Cannon digital camera and has 5184 pixels in the x direction and 3456 pixels in the y direction. The ruler in the photo reflects the actual scale of the geomaterials and indicates that each pixel has a length of 0.125 mm.

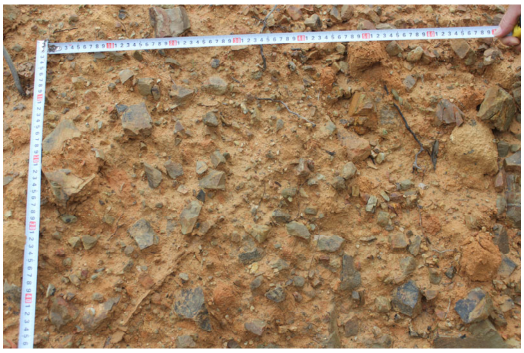

Fig. 2 A photograph of a soil and rock mixture

The photograph was taken in Donglingxin landslide accumulation mass of Sanbanxi Hydropower Station in Jianhe County of Guizhou Province, China on May 16, 2014. The accumulated mass was composed mainly of the residual deposits, sliding deposits, silty clay, and crushed stone soil, and fractured rock mass typical of the soil and rock mixture.

2.1 Noise removal

Noise is inevitable in the acquisition of digital images. There are lots of ways to generate noise, and the sources can be divided into two categories, namely environmental factors and internal factors. For example, sunshine and parameters of the camera affect the quality of images. Noise will influence the extraction of microstructural information from geomaterial images. Hence, noise removal methods are basic processes in the pre-treatment of images. There are several commonly used techniques including neighborhood averaging, wavelet denoising, and lower pass filtering methods. Considering that some noise removal methods may blur edges and lose other information, an easy yet effective method, the median method, was used in this study. This method was also used by Yue *et al.* (2003).

To eliminate the effect of measuring tape, we chose a part of Fig. 2 as the research domain (Fig. 3). In the following section, we propose a systematic procedure for the treatment of color images.

Median filtering is a type of non-linear smoothing method which can keep the boundaries of original figures clear. For a square with a size of 3×3 or 5×5 pixels, the equation of the function of the medium filter $g(i, j)$ can be written simply as

$$g(i,\ j) = \text{median}\left\{ f(i-K,\ j-I),\ (K, I \in W) \right\}, \quad (2)$$

where W is the neighboring window.

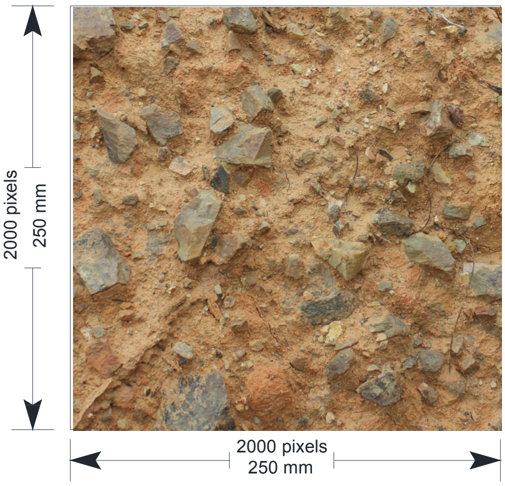

Fig. 3 The domain of the photo used for research

In this study, a simple neighboring window, a square with a size of 3×3 pixels, was used. The programs for the median filter and other related procedures were written using MATLAB. Fig. 4 shows the image results before and after noise removal. Only a small part of the original figure was taken as the example because the effects of noise may be hidden at low magnification. Compared with the original figure (Fig. 4a), the new figure (Fig. 4b) is clearer and the noise points have been removed.

2.2 Color space conversion

Digital images produced by most scanners and cameras are colored figures characterized by a certain color space and multi-dimensional arrangements. Because all colors can be regarded as a combination of red (R), green (G), and blue (B), the RGB color space is the most frequently used in applications in our daily life. Although the RGB color system can be recognized by human eyes, it is not as effective as the hue (H) saturation (S) intensity (I) (HSI) color space in terms of image recognition for computer programs. The HSI color space can be described by a circular cone model (Fig. 5) (Sharma and Bala, 2002). Though the expression of the HSI color space is very complex, it gives a more precise description of a color image. The properties of the HSI model make it well suited for the analysis of color figures.

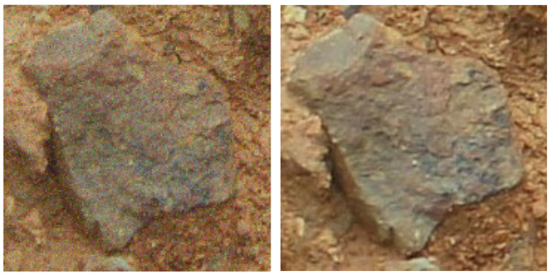
(a) (b)

Fig. 4 Effects of a median filter in the pre-treatment of a color image: (a) original image with noise; (b) image after applying the median filter

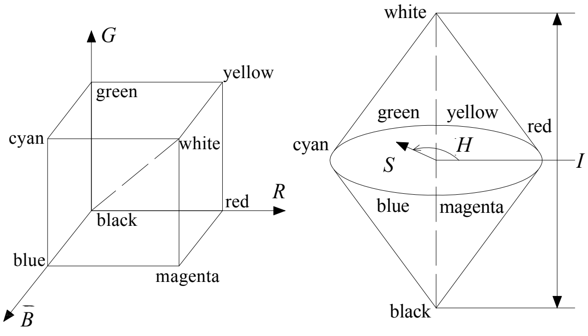

(a) (b)

Fig. 5 RGB (a) and HSI (b) color space models

For the convenience of digital analysis, we need to transfer images from the RGB model to the HSI model. The essence of this process is the transition from a unit cube under Cartesian coordinate to a bi-pyramid in the cylindrical coordinate. The simplest transformation is presented as follows.

$$H=\begin{cases}\theta, & G\geq B,\\ 2\pi-\theta, & G<B,\end{cases} \tag{3}$$

$$S=1-\frac{3\min(R,G,B)}{R+G+B},\quad I=\frac{R+G+B}{3},$$

where

$$\theta=\cos^{-1}\left[\frac{(R-G)+(R-B)}{2\sqrt{(R-G)^2+(R-G)(R-B)}}\right].$$

Other methods like coordinate transition, Bajon approximation, and piecewise definition can also be applied (Haralick and Shapiro, 1991).

A MATLAB program rgb2hsi (Gonzalez *et al.*, 2009) was employed in the digital analysis of the image of geomaterials. The three components of the HSI color model were determined (Fig. 6). Differences between soil and rock in hue and intensity are not evident, while those in saturation are obvious. Therefore, we are able to distinguish rocks in the image based on saturation.

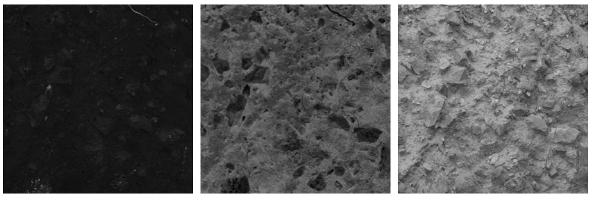
(a) (b) (c)

Fig. 6 HSI components grayscale of the image of the SRM: (a) hue; (b) saturation; (c) intensity

2.3 Image binaryzation

A clustering-based method for binaryzation was used in this study. The threshold is taken as the value where the gray-level samples are clustered in two parts as background and foreground (Sezgin and Sankur, 2004). For a figure with two peaks, the threshold is the lowest point between the peaks, and for a figure with one peak, the threshold is the peak value.

According to the above analysis, we take the grayscale of the saturation as the factor differentiating rocks and soil. The determination of the proper threshold is very important. A histogram of saturation values in HSI color space is shown in Fig. 7. From the histogram of the S component, as the value of saturation increases up to 0.27, the frequency grows continuously, and then after the peak it falls gradually. Therefore, we set the value of the threshold as 0.27 for binaryzation. The final binary image is shown in Fig. 8a, where the rock aggregates can be identified.

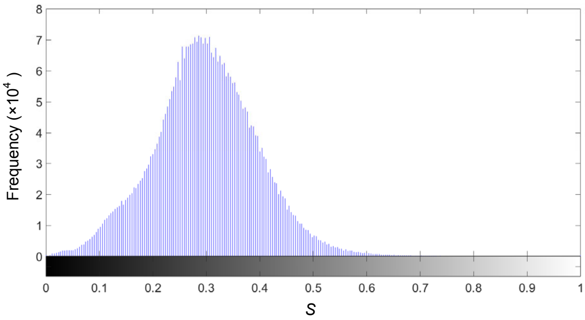

Fig. 7 Histogram of *S* values in the HSI color space

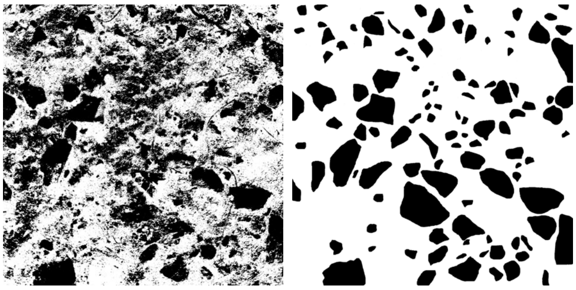
(a) (b)

Fig. 8 Automatic binary image (a) and manual refinement binary image (b)

Since the distinction between soil and rocks is not evident and sometimes rock surfaces are covered by soil, manual refinements are needed based on the human eye view. We can modify the image with the help of software packages such as Photoshop or Painter. In the binary image, 0 represents black while 1 represents white, and a transformation of 0 and 1 is applied. The final result of the microstructure of the SRM is shown in Fig. 8b. The next section will focus on the vectorization of binary images using a novel method.

3 Microstructure analysis and geometry vectorization of the binary image

3.1 Connected-component labeling algorithm

The distribution of rocks in the SRM can be seen in Fig. 8. A quantitative analysis of the properties of each rock has still not been achieved. From the binary image, we see that all the pixels in an aggregate are adjacent to each other, hence each rock can be regarded as a connected component. Therefore, we use a connected component labeling algorithm to tackle this problem.

A component labeling algorithm is a fundamental image processing technique which segments the domain of a binary image into partitions corresponding to connected components (Wilson and Ritter, 2000). For binary images, a unique number is first assigned to each blob. If each blob corresponds to a single object, objects that exist in a binary image are counted. Generally speaking, labeling algorithms can be divided into two large classes: (a) local neighborhood algorithms and (b) divide-and-conquer algorithms (Pitas, 2000). For the local neighborhood algorithms, we often use 4- or 8-connectivity in component labeling. Taking a simple binary image as an example, the results of 4- and 8-connectivity labeling are listed in Fig. 9. For identification of different rocks, we use an 8-connectivity labeling algorithm and analyze statistical information on the distribution of the aggregates based on the results of labeling.

1	1	1	0	0	0	0	0
1	1	1	0	2	2	0	0
1	1	1	0	2	2	0	0
1	1	1	0	0	0	2	0
1	1	1	0	0	0	2	0
1	1	1	0	0	0	2	0
1	1	1	0	0	2	2	0
1	1	1	0	0	0	0	0

(a)

1	1	1	0	0	0	0	0
1	1	1	0	1	1	0	0
1	1	1	0	1	1	0	0
1	1	1	0	0	0	1	0
1	1	1	0	0	0	1	0
1	1	1	0	0	0	1	0
1	1	1	0	0	1	1	0
1	1	1	0	0	0	0	0

(b)

1	1	1	0	0	0	0	0
1	1	1	0	1	1	0	0
1	1	1	0	1	1	0	0
1	1	1	0	0	0	1	0
1	1	1	0	0	0	1	0
1	1	1	0	0	0	1	0
1	1	1	0	0	1	1	0
1	1	1	0	0	0	0	0

(c)

Fig. 9 A simple illustration of the connected-component labeling algorithm

(a) original binary data; (b) result of 8-connectivity labeling; (c) result of 4-connectivity labeling

3.2 Geometry vectorization of the binary image

3.2.1 Edge extraction

Edge detection is an essential procedure in the vectorization of binary images. Yue *et al.* (2003) used first-order derivatives and modified the results manually with Photoshop. We propose a more efficient method using the connected-component labeling algorithm. We consider one pixel as a square with four sides. As for a connected-component with a size of N pixels, there are $4\times N$ sides in total. If a side is at the edge of the domain, it will be unique while other sides will repeat twice. If we delete all the sides which repeat twice, the remainders are the scattered edges of connected-components. After we obtain the scattered lines, the edges need to be connected in sequential order.

Taking two adjacent pixels A and B as an example, the four sides of pixel A are p_1-p_2, p_1-p_3, p_2-p_4, and p_3-p_4 and those of pixel B are p_2-p_5, p_2-p_4, p_5-p_6, and p_4-p_6. It is easy to delete the repeated side p_2-p_4. The remaining sides are the edges. We choose an arbitrary point as the beginning, then the next point can be determined by the connection relationship. For example, if the starting point is p_1, the next point is p_2 or p_3 according to the lines p_1-p_2 and p_1-p_3. Assuming the second point is p_2, the next point is p_5. In this way, a closed polyline p_1-p_2-p_5-p_6-p_4-p_3-p_1 is obtained (Fig. 10). Based on this consideration, we developed a computer program to extract the edges of the rocks (Fig. 11a).

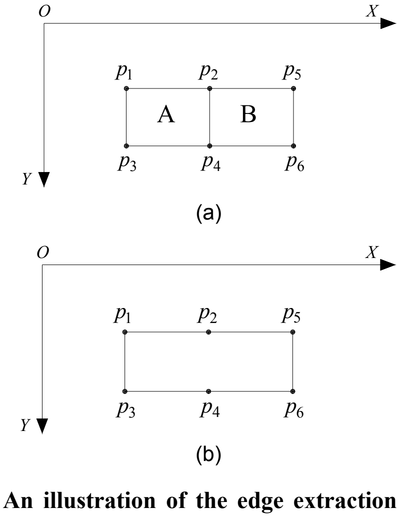

Fig. 10 An illustration of the edge extraction technique used in this study: (a) original connected component; (b) edge of the domain

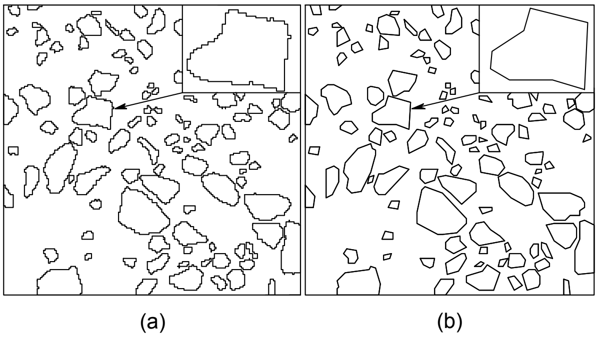

Fig. 11 Edge detection of the rocks in the SRM: (a) edge extraction without boundary smoothing; (b) edge extraction after boundary smoothing

3.2.2 Boundary processing and transformation for vectorial file

After the extraction of the edges, the boundaries of the rock appear jagged and do not reflect the real edges of the rocks. Also, excessive numbers of nodes make the generation of computational models difficult. Hence, a boundary processing method proposed by Yue *et al.* (2003) was applied in this study. The method is briefly explained as follows:

1. Set a threshold value T.

2. Find two points separated by the longest distance and link them to separate the polyline into two parts.

3. For a random part, calculate the maximum perpendicular distance of all points. If the maximum distance is greater than T, divide this part into two segments. Link this point and the former two points.

4. Repeat this process until the distance of all the segments is less than T.

With the help of this technique, we set the threshold value T as 10. The results show that this method can reduce the number of points on rocks (Fig. 11b). After the acquisition of the boundary information, a scale transition is needed. Because pixel information is made up of integer variables and the actual size corresponding to each pixel is known, we simply multiply the location of each point in the image by the length of each pixel to obtain the size of the SRM measured in centimetre or millimetre.

For the convenience of later analysis, we import the information from these edges into a vectorial file. Due to the wide usage of AutoCAD in engineering, we chose Drawing Interchange Format (DXF) as the vectorization format. Finally, based on the data structure of DXF, we put the geometry information of the SRM into a DXF file, which is helpful for both mesh generation and statistical analysis of rock information.

3.3 Distribution information of microstructures

Having described the DIP method used in this study, we can obtain the statistical information relating to rock size using a connected-component labeling algorithm and distribution information, such as rose diagrams of rocks in the SRM. This process is written into a computer program and the rock statistics obtained can be seen in Table 1 and Fig. 12. The proportion of rock was 41.52%, the majority of which consisted of large rocks. The result shows that the connected-component labeling algorithm is efficient for the analysis of the distribution of components in an SRM.

Table 1 Statistical information regarding the distribution of rocks in an SRM

Rock area (mm^2)	Rocks number	Rock area (mm^2)	Area ratio (%)
0–50	39	1236	3.09
51–100	29	2016	5.04
100–200	17	2474	6.19
200–500	18	5722	14.31
500–2000	7	5159	12.90
Total	110	16 607	41.52

4 Application of DIP to seepage analysis

4.1 Finite element mesh generation

Automatic generation of grids for finite element analysis has been a popular topic associated with the boom in the development of numerical methods. There are a lot of techniques for generating finite element grids. The three most widely used are the quadtree-octree based method, advancing front method, and Delaunay based method (Frey and George, 2010). Nowadays, developments of FEM, such as arbitrary-Lagrangian-Eulerian (ALE), bring new mesh requirements like adaptation and moving techniques. In this study, the requirements for the grid are simple, and conventional techniques are sufficient.

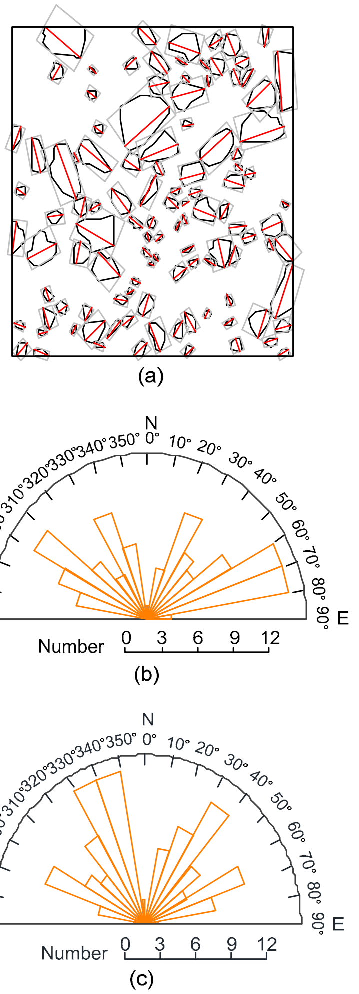

Fig. 12 Rose diagram of rock aggregates in the SRM: (a) major and minor axes of rock aggregates; (b) major axis rose diagram; (c) minor axis rose diagram

There are many commercial and open source software programs, including Ansys, HyperWorks, and Gmsh, that can mesh a finite element grid automatically. By importing vectorized image files, these software programs can easily generate the mesh. The final mesh for the analysis is shown in Fig. 13.

4.2 Numerical permeability test

Many numerical solutions for the seepage problem have been proposed (Smith *et al.*, 2013; Zienkiewicz *et al.*, 2013). Therefore, a detailed introduction will not be provided here. To analyze the seepage properties of SRMs, a numerical permeability test was employed. The laboratory seepage experiment is illustrated in Fig. 14. For the numerical test, we set the boundary condition the same as that in the laboratory. The water head difference (Δh) was 1 m, the width (A) of the specimen 229.1 mm, and the height (L) 166.5 mm. The permeability parameters for different composites were taken from suggestions in the engineering geology handbook (Table 2) (Chang and Zhang, 2007). It is clear that the rock aggregate and the soil matrix have different permeability coefficients, but there have been few studies about the seepage properties of this heterogeneous material.

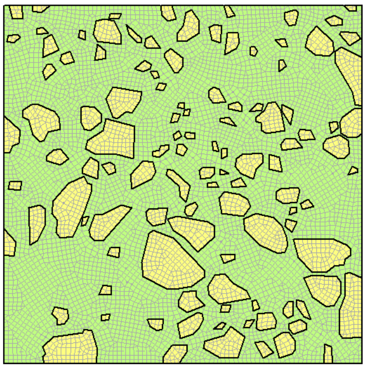

Fig. 13 Finite element mesh of the SRM

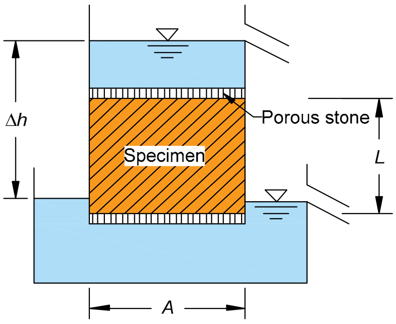

Fig. 14 Illustration of the laboratory permeability experiment with a constant water level

Table 2 Suggested permeability coefficients for the soil and rock components (Chang and Zhang, 2007)

Component	Permeability coefficient (mm/s)
Soil	3.0×10^{-3}
Rock	5.0×10^{-5}

To reflect the effects of the heterogeneity, a homogeneous reference with a permeability coefficient of 3.0×10^{-3} mm/s was set. The water pressure fields after the finite element analysis are shown in Fig. 15. From the contour of the total head, we can see there is a difference between the homogeneous and heterogeneous media. The water pressure isocline in the homogeneous medium has a uniform horizontal distribution, while that in the SRM is non-uniform. We monitored the pore pressure of two vertical lines of the heterogeneous specimen at X=50 mm and X=150 mm, where X is the horizontal coordinate. The relationship between the total head and vertical coordinate (Y) for the homogeneous and heterogeneous media is demonstrated in Fig. 16.

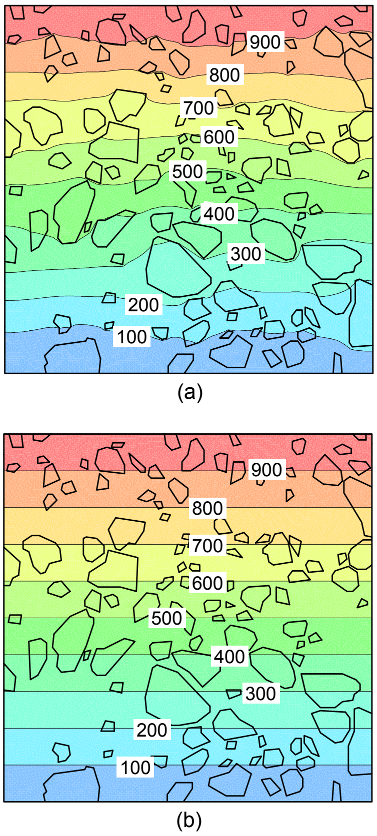

(a)

(b)

Fig. 15 Total head contour of heterogeneous (a) and homogeneous (b) media (unit: mm)

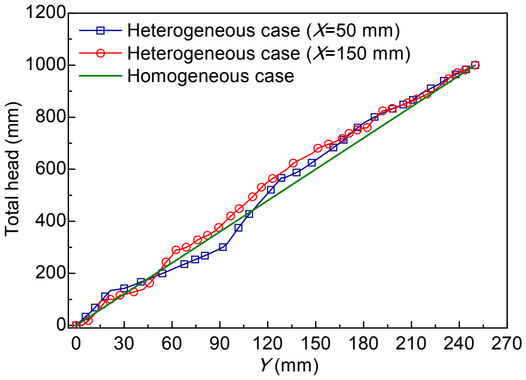

Fig. 16 Relationship between total head and vertical coordinate

Considering the total head contour cannot intuitively reflect the heterogeneity, a plot of hydraulic velocity vectors for homogeneous and heterogeneous media is proposed (Fig. 17). The flow velocities in the rock and soil are different, and the flow velocity in the rock is nearly zero. As a result, the macro permeability varies among different mesostructures. To evaluate the macro permeability of the SRM, we recorded the flux in the numerical experiment. The flux Q was 4.128 ml/s in the homogeneous medium and 1.63 ml/s in the SRM. The formula for the permeability coefficient k for a constant water level experiment is

$$k=\frac{QL}{A\Delta h}. \tag{4}$$

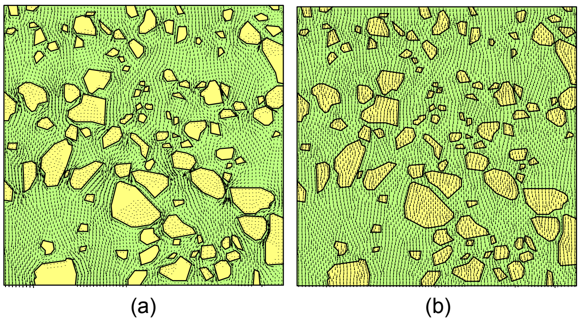
(a) (b)

Fig. 17 Flux velocity vectors for heterogeneous (a) and homogeneous (b) media

Based on the simple equation above, the macro permeability coefficient was obtained. The results for the two numerical specimens were 3.00×10^{-3} mm/s and 1.63×10^{-3} mm/s. Due to the effects of rock aggregate with a low coefficient parameter, the macro permeability coefficient showed a clear decline. The coefficient in the homogeneous medium was the same as the soil parameter, which indicates that the result from the numerical experiment was reasonable.

5 Results and discussion

Turning to the effect of the mesostructure on permeability, with the help of the method described in this paper, the macro permeability coefficient for heterogeneous media in different mesostructures can be estimated. The results from three perspectives are discussed as follows.

5.1 Scale dependency and representative element volume estimation

As for the heterogeneous materials, the equivalent physical parameters have scale dependency. Only when it is larger than the representative element volume (REV), will the scale have little influence on physical parameters. The determination of REV for SRM is a rather subjective task that involves estimating how many pixels are needed. Random sampling is chosen for the estimation of the permeability coefficient at different scales (Fig. 18). Rocks in the SRM become small, and the material tends to be homogeneous as the scale increases. We employed four random tests at each scale, and the results are shown in Fig. 19.

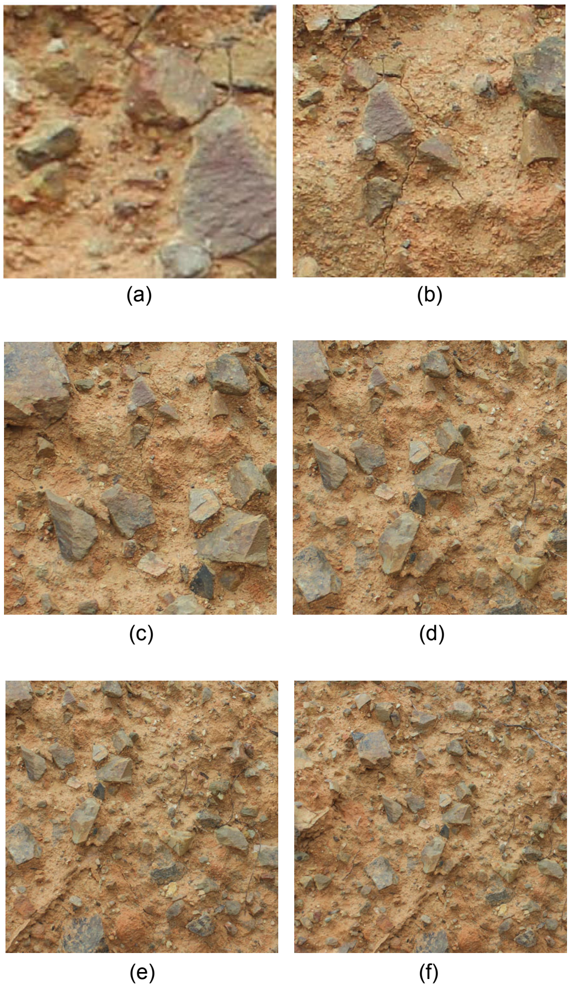
(a) (b) (c) (d) (e) (f)

Fig. 18 Random domain at different scales

(a) 2002 pixels; (b) 5002 pixels; (c) 10 002 pixels; (d) 15 002 pixels; (e) 20 002 pixels; (f) 25 002 pixels

Fig. 19 clearly illustrates the scale dependency of the permeability of the SRM. The permeability coefficient to be estimated can have a wide range within a certain scale. In these cases, beyond a scale of 2500 pixels, corresponding to a length of about 300 mm, the scattering range of the properties becomes notably smaller and the material can be regarded as homogeneous. As the largest axis of rock aggregate is 49 mm, the REV length is about six times the maximum major axis of aggregate. For the simulation of heterogeneous media using digital images, a proper large scale is required to obtain reliable results.

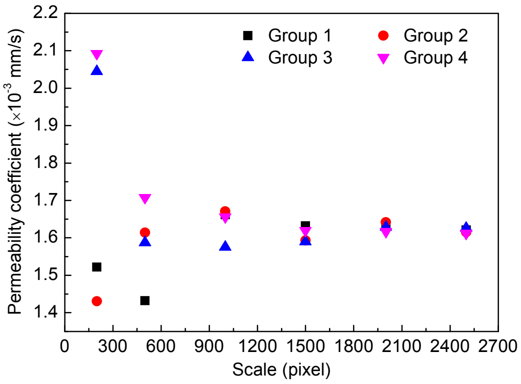

Fig. 19 Variation in permeability coefficient with the increasing numbers of pixels

5.2 Effect of the material property on macro permeability

Having analyzed the scale dependency of the SRM, we analyze the effect of the rock coefficient on macro permeability. Firstly, we denote a parameter (λ) which represents the heterogeneity of the material. The permeability coefficients associated with different heterogeneity parameters are listed in Table 3.

Fig. 20 shows the variation in macro permeability k_{macro} with the heterogeneity parameter λ. It shows that the macro permeability k_{macro} decreases as the heterogeneity parameter λ increases from 1 to 100. Before λ reaches the value of 20, the variation in macro permeability is obvious. The change of macro permeability slows down once λ reaches 20. This indicates that heterogeneity has a large influence on macro permeability, especially when the differences among components in heterogeneous geomaterials are not significantly large.

Table 3 Permeability coefficients associated with different heterogeneity parameters

Case	k_{soil} (mm/s)	k_{rock} (mm/s)	λ	k_{macro} (mm/s)
1	3.0×10^{-3}	1.5×10^{-3}	2	2.51×10^{-3}
2	3.0×10^{-3}	6.0×10^{-4}	5	2.06×10^{-3}
3	3.0×10^{-3}	3.0×10^{-4}	10	1.85×10^{-3}
4	3.0×10^{-3}	1.5×10^{-4}	20	1.72×10^{-3}
5	3.0×10^{-3}	6.0×10^{-5}	50	1.64×10^{-3}
6	3.0×10^{-3}	3.0×10^{-5}	100	1.61×10^{-3}

k_{soil} and k_{rock} represent the permeability coefficients of soil and rock, respectively; $\lambda=k_{\text{soil}}/k_{\text{rock}}$

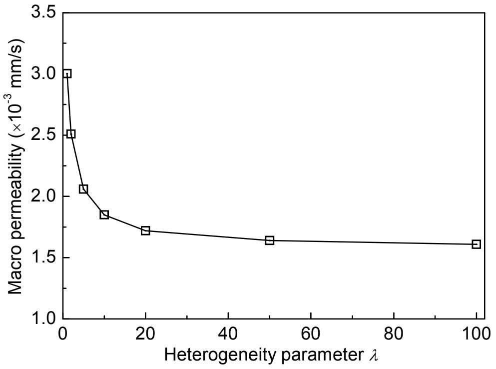

Fig. 20 Variation in macro permeability k_{macro} with the heterogeneity parameter λ

5.3 Effect of the rock fraction on macro permeability

To analyze the influence of the rock fraction on the macro equivalent permeability of the SRM, we take another three photos of SRMs with different rock fractions. The numerical models of these tests are shown in Fig. 21. According to the numerical analysis, the macro permeability and the corresponding rock fractions are shown in Table 4.

The macro permeability tends to decrease as the rock fraction increases. However, the rock fraction is

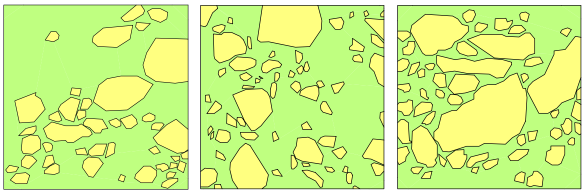
(a) (b) (c)

Fig. 21 Numerical tests of SRMs with different rock fractions: (a) 30.20%; (b) 33.40%; (c) 50.97%

Table 4 Permeability coefficients with different rock fractions

Test No.	Rock fraction (%)	Macro permeability ($\times 10^{-3}$ mm/s)
1	30.20	1.80
2	33.40	1.48
3	41.52	1.63
4	50.97	0.51

not the only factor that affects the macro permeability. In the cases analyzed above, the macro permeability with a rock fraction of 30.20% is larger than that with a rock fraction of 33.40%. The distribution and shapes are also very important in determining the macro permeability property of an SRM.

6 Conclusions

This paper establishes a numerical method based on DIP for analyzing the permeability of geomaterials, considering the materials' heterogeneity. First, we summarized the basic features of DIP, such as noise removal, color space conversion, and image binaryzation. By introducing the connected-component labeling algorithm, a novel, simple, yet effective method for the geometry vectorization of a photograph is presented. Using a photo of an SRM as an example, we demonstrated the implementation of this method in the permeability analysis of heterogeneous materials. The feasibility and rationality of this method was shown by *in-situ* tests and numerical analysis. Furthermore, we analyzed the effects of heterogeneity on macro permeability from three perspectives:

1. By a series of numerical analyses at different scales from 2002 pixels to 25002 pixels, we showed that the SRM had scale dependency, and the REV size was about six times the maximum major axis length.

2. Analyses of the variation in macro permeability associated with heterogeneity parameters were carried out, and the results showed that their effects were notable within a certain range.

3. Simulations of the effect of different rock fractions on permeability showed that increasing the rock fraction can reduce macro permeability. However, the distribution and shape of the aggregate should also be taken into consideration.

In this paper, we proposed a novel method for evaluating macro permeability at an *in-situ* scale to provide a prognosis for engineers. This method can be applied to the analysis of other heterogeneous media and related problems associated with microstructure. Although this study dealt with a 2D simulation, the method could be extended to 3D analysis.

References

Ammouche, A., Breysse, D., Hornain, H., *et al.*, 2000. A new image analysis technique for the quantitative assessment of microcracks in cement-based materials. *Cement and Concrete Research*, **30**(1):25-35. http://dx.doi.org/10.1016/S0008-8846(99)00212-4

Armesto, J., Lubowiecka, I., Ordóñez, C., *et al.*, 2009. FEM modeling of structures based on close range digital photogrammetry. *Automation in Construction*, **18**(5):559-569. http://dx.doi.org/10.1016/j.autcon.2008.11.006

Bažant, Z.P., Tabbara, M.R., Kazemi, M.T., *et al.*, 1990. Random particle model for fracture of aggregate or fiber composites. *Journal of Engineering Mechanics*, **116**(8): 1686-1705. http://dx.doi.org/10.1061/(ASCE)0733-9399(1990)116:8(1686)

Bessa, I.S., Branco, V.T.C., Soares, J.B., 2012. Evaluation of different digital image processing software for aggregates and hot mix asphalt characterizations. *Construction and Building Materials*, **37**:370-378. http://dx.doi.org/10.1016/j.conbuildmat.2012.07.051

Carroll, J.D., Abuzaid, W., Lambros, J., *et al.*, 2013. High resolution digital image correlation measurements of strain accumulation in fatigue crack growth. *International Journal of Fatigue*, **57**(12):140-150. http://dx.doi.org/10.1016/j.ijfatigue.2012.06.010

Chang, S., Zhang, S., 2007. Engineering Geology Handbook. China Architecture & Building Press, Beijing, China (in Chinese).

Chaves, A., La Scalea, R., Colturato, A., *et al.*, 2015. Using UAVs and digital image processing to quantify areas of soil and vegetation. *Journal of Physics: Conference Series*, **633**(1):012112. http://dx.doi.org/10.1088/1742-6596/633/1/012112

Chen, S., Yue, Z., Tham, L., 2004. Digital image-based numerical modeling method for prediction of inhomogeneous rock failure. *International Journal of Rock Mechanics and Mining Sciences*, **41**(6):939-957. http://dx.doi.org/10.1016/j.ijrmms.2004.03.002

Chen, S., Yue, Z.Q., Tham, L.G., 2005. Digital image based numerical modeling method for heterogeneous geomaterials. *Chinese Journal of Geotechnical Engineering*, **27**(8):956-964.

Chen, S., Yue, Z.Q., Tham, L.G., 2007. Digital image based approach for three-dimensional mechanical analysis of heterogeneous rocks. *Rock Mechanics and Rock Engineering*, **40**(2):145-168. http://dx.doi.org/10.1007/s00603-006-0105-8

Chena, S., Yueb, Z.Q., Kwan, A., 2013. Actual microstructure-based numerical method for mesomechanics of concrete. *Computers and Concrete*, **12**(1):1-18. http://dx.doi.org/10.12989/cac.2013.12.1.001

Frey, P.J., George, P.L., 2010. Mesh Generation. John Wiley & Sons, New York, USA.

Gonzalez, R.C., Woods, R.E., Eddins, S.L., 2009. Digital Image Processing Using MATLAB, 2nd Edition. Publishing House of Electronics Industry, Beijing, China.

Haralick, R.M., Shapiro, L.G., 1991. Glossary of computer vision terms. *Pattern Recognition*, **24**(1):69-93. http://dx.doi.org/10.1016/0031-3203(91)90117-N

Johnson, N.L., Kotz, S., Balakrishnan, N., 2002. Continuous Multivariate Distributions: Volume 1, Models and Applications. John Wiley & Sons, New York, USA.

Kameda, A., 2004. Permeability Evolution in Sandstone: Digital Rock Approach. PhD Thesis, Stanford University, CA, USA.

Kemeny, J., Mofya, E., Kaunda, R., *et al.*, 2010. Improvements in blast fragmentation models using digital image processing. *Fragblast*, **6**(3):311-320. http://dx.doi.org/10.1076/frag.6.3.311.14051

Khan, M.B., Xue, Y.L., Nisar, H., *et al.*, 2015. Digital image processing and analysis for activated sludge wastewater treatment. *Advances in Experimental Medicine & Biology*, **823**:227-248. http://dx.doi.org/10.1007/978-3-319-10984-8_13

Kwan, A.K.H., Wang, Z.M., Chan, H.C., 1999a. Mesoscopic study of concrete II: nonlinear finite element analysis. *Computers & Structures*, **70**(5):545-556. http://dx.doi.org/10.1016/S0045-7949(98)00178-3

Kwan, A.K.H., Mora, C.F., Chan, H.C., 1999b. Particle shape analysis of coarse aggregate using digital image processing. *Cement and Concrete Research*, **29**(9):1403-1410. http://dx.doi.org/10.1016/S0008-8846(99)00105-2

Li, A., Shao, G.J., Yu, T.T., *et al.*, 2014. Mesoscopic numerical simulation of stratified rock failure using digital image processing. *Advances in Mechanical Engineering*, **2014**(12):1-12. http://dx.doi.org/10.1155/2014/106073

Mariño, A., Luthin, J.N., 1982. Seepage and Groundwater. Elsevier Science, the Netherlands.

Michailidis, N., Stergioudi, F., Omar, H., *et al.*, 2010. An image-based reconstruction of the 3D geometry of an Al open-cell foam and FEM modeling of the material response. *Mechanics of Materials*, **42**(2):142-147. http://dx.doi.org/10.1016/j.mechmat.2009.10.006

Pitas, I., 2000. Digital Image Processing Algorithms and Applications. John Wiley & Sons, New York, USA.

Rushton, K.R., 2004. Groundwater Hydrology: Conceptual and Computational Models. John Wiley & Sons, New York, USA.

Sezgin, M., Sankur, B., 2004. Survey over image thresholding techniques and quantitative performance evaluation. *Journal of Electronic Imaging*, **13**(1):146-168. http://dx.doi.org/10.1117/1.1631315

Sharma, G., Bala, R., 2002. Digital Color Imaging Handbook. Taylor & Francis, UK.

Skoczylas, F., Henry, J.P., 1995. A study of the intrinsic permeability of granite to gas. *International Journal of Rock Mechanics and Mining Sciences & Geomechanics Abstracts*, **32**(2):171-179. http://dx.doi.org/10.1016/0148-9062(94)00022-U

Smith, I.M., Griffiths, D.V., Margetts, L., 2013. Programming the Finite Element Method. John Wiley & Sons, New York, USA.

Steinberg, E., Prilutsky, Y., Corcoran, P., *et al.*, 2010. Digital Image Processing Using Face Detection Information. US Patent 7574016.

Venkatramaiah, C., 2006. Geotechnical Engineering. New Age International (P) Limited, New Delhi, India.

Wang, X.F., Yang, Z.J., Yates, J., *et al.*, 2015. Monte Carlo simulations of mesoscale fracture modelling of concrete with random aggregates and pores. *Construction and Building Materials*, **75**:35-45. http://dx.doi.org/10.1016/j.conbuildmat.2014.09.069

Wang, Z.M., Kwan, A., Chan, H.C., 1999. Mesoscopic study of concrete I: generation of random aggregate structure and finite element mesh. *Computers & Structures*, **70**(5):533-544. http://dx.doi.org/10.1016/S0045-7949(98)00177-1

Wilson, J.N., Ritter, G.X., 2000. Handbook of Computer Vision Algorithms in Image Algebra. Taylor & Francis, UK.

Xu, J.M., Zhao, X.B., Liu, B., 2007. Digital image analysis of fluid inclusions. *International Journal of Rock Mechanics and Mining Sciences*, **44**(6):942-947. http://dx.doi.org/10.1016/j.ijrmms.2007.01.003

Xu, W.J., Hu, R.L., Wang, Y.P., 2007. PFC^{2D} model for mesostructure of inhomogeneous geomaterial based on digital image processing. *Journal of China Coal Society*, **32**(4):358-362 (in Chinese).

Xu, W.J., Hu, R.L., Yue, Z.Q., 2008a. Meso-structure character of soil-rock mixtures based on digital image. *Journal of Liaoning Technical University (Natural Science)*, **27**(1):51-53 (in Chinese).

Xu, W.J., Yue, Z.Q., Hu, R.L., 2008b. Study on the mesostructure and mesomechanical characteristics of the soil–rock mixture using digital image processing based finite element method. *International Journal of Rock Mechanics and Mining Sciences*, **45**(5):749-762. http://dx.doi.org/10.1016/j.ijrmms.2007.09.003

Xu, Y., Gao, Q., Li, X., *et al.*, 2009. *In-situ* experimental study of permeability of rock and soil aggregates. *Rock and Soil Mechanics*, **30**(3):855-858 (in Chinese).

Yu, Q.L., Tang, C.A., Zhu, W.C., *et al.*, 2006. Digital image processing based modeling of rock failure in meso-scale.

Mechanics in Engineering, **28**(4):60-64.
http://dx.doi.org/10.6052/1000-0992-2005-339

Yu, Q.L., Tang, C.A., Tang, S.B., 2007. Digital image based characterization method of rock's heterogeneity and its primary application. *Chinese Journal of Rock Mechanics & Engineering*, **26**(3):551-559 (in Chinese).

Yu, Q.L., Zheng, C., Yang, T.H., *et al.*, 2012. Meso-structure characterization based on coupled thermal-mechanical model for rock failure process and applications. *Chinese Journal of Rock Mechanics & Engineering*, **31**(1):42-51 (in Chinese).

Yue, Z.Q., Bekking, W., Morin, I., 1995. Application of digital image processing to quantitative study of asphalt concrete microstructure. *Transportation Research Record*, **1492**: 53-60.

Yue, Z.Q., Chen, S., Tham, L., 2003. Finite element modeling of geomaterials using digital image processing. *Computers and Geotechnics*, **30**(5):375-397.
http://dx.doi.org/10.1016/S0266-352X(03)00015-6

Yue, Z.Q., Chen, S., Zheng, H., *et al.*, 2004. Digital image proceeding based on finite element method for geomaterials. *Chinese Journal of Rock Mechanics and Engineering*, **23**(6):889-897 (in Chinese).

Zeng, Q.L., Wang, J.G., Wang, L., *et al.*, 2013. The research of coal mine conveyor belt tearing based on digital image processing. Proceedings of the 2012 International Conference on Communication, Electronics and Automation Engineering, p.187-191.
http://dx.doi.org/10.1007/978-3-642-31698-2_27

Zhou, Z., Fu, H.L., Liu, B.C., *et al.*, 2006. Experimental study of the permeability of soil-rock-mixture. *Journal of Hunan University (Natural Sciences)*, **33**(6):25-28 (in Chinese).

Zhu, W.C., Kang, Y.M., Yang, T.H., *et al.*, 2006. Application of digital image-based heterogeneity characterization in coupled hydromechanics of rock. *Chinese Journal of Geotechnical Engineering*, **28**(12):2087-2091 (in Chinese).

Zienkiewicz, O.C., Taylor, R.L., Zhu, J.Z., 2013. The Finite Element Method: Its Basis and Fundamentals. Elsevier Science, the Netherlands.

中文概要

题　目：基于数字图像的非均匀岩土材料渗透系数研究

目　的：建立一种较为快速和快速确定非均匀岩土材料渗透系数的方法。

创新点：建立了一种可以从图像到数值模型的数字图像方法：通过拍照、CT 等手段获取岩土材料的图像，进而通过数值分析确定等效参数。

方　法：1. 将采集到彩色图像从 RGB 空间转化到 HSI 空间，选取识别度较高的空间进行二值化处理；2. 获取二值化图像后采用邻域标记算法标记，结合本文提出的算法提取边界（图 9 和 10）；3. 结合边界修正算法对锯齿状边界进行修正（图 11）；4. 确定表征细观几何模型（图 12 和表 1）；5. 绘制网格开展数值分析，确定宏观参数。

结　论：1. 基于数值图像的非均匀岩土材料渗透系数确定方法可以较为准确地估算渗透系数，可以为工程设计提供初步依据。2. 非均匀岩土材料具有明显的尺寸效应，随着尺寸增加，渗透率的变化逐渐趋于稳定；当材料视为岩石和土体的二元介质时，两种性质差异在 10 倍以内对宏观特性的影响较大，大于 10 倍之后影响减弱。3. 岩土材料渗透率随着内部块石含量的增加而减小，但是内部块石的形态对渗透率也有一定的影响。

关键词：非均质岩土材料；数字图像；宏观渗透系数；尺寸效应